



LAWRENCE
LIVERMORE
NATIONAL
LABORATORY

The National Ignition Facility (NIF) Diagnostic Set at the Completion of the National Ignition Campaign (NIC) September 2013

J. Kilkenny, P. E. Bell, D. K. Bradley, D. L. Bleuel, J. A. Caggiano, E. L. Dewald, W. Hsing, H. Kalantar, R. Kauffman, J. D. Moody, M. B. Schneider, D. A. Shaughnessy, R. T. Shelton, C. B. Yeaman, S. H. Batha, G. P. Grim, H. W. Herrmann, F. E. Merrill, R. J. Leeper, T. C. Sangster, D. H. Edgell, V. Yu Glebov, S. P. Regan, J. A. Frenje, M. Gatu-Johnson, R. D. Petrasso, H. G. Rindernecht, A. B. Zylstra, G. W. Cooper, C. Ruiz

January 22, 2015

Disclaimer

This document was prepared as an account of work sponsored by an agency of the United States government. Neither the United States government nor Lawrence Livermore National Security, LLC, nor any of their employees makes any warranty, expressed or implied, or assumes any legal liability or responsibility for the accuracy, completeness, or usefulness of any information, apparatus, product, or process disclosed, or represents that its use would not infringe privately owned rights. Reference herein to any specific commercial product, process, or service by trade name, trademark, manufacturer, or otherwise does not necessarily constitute or imply its endorsement, recommendation, or favoring by the United States government or Lawrence Livermore National Security, LLC. The views and opinions of authors expressed herein do not necessarily state or reflect those of the United States government or Lawrence Livermore National Security, LLC, and shall not be used for advertising or product endorsement purposes.

This work performed under the auspices of the U.S. Department of Energy by Lawrence Livermore National Laboratory under Contract DE-AC52-07NA27344.

The National Ignition Facility (NIF) Diagnostic Set at the Completion of the National Ignition Campaign (NIC) September 2013

J. D. Kilkenny, General Atomics
P. E. Bell , D. K. Bradley, D. L. Bleuel ,J. A. Caggiano, E. L. Dewald W.W. Hsing, D.
H. Kalantar, R. L. Kauffman, J. D. Moody, M.B. Schneider, D. A. Shaughnessy, R.
T. Shelton, C. B. Yeamans, LLNL
S.H. Batha, G. P. Grim, H. W. Herrmann, F. E. Merrill, R. J. Leeper, LANL
T. C. Sangster, D. H. Edgell , V Yu Glebov, S. P. Regan LLE
J.A. Frenje, M. Gatu-Johnson, R. D.Petrasso , H. G. Rindernecht, A.B. Zylstra,
MIT
G. W. Cooper, C. Ruiz SNL

Abstract:

At the completion of the National Ignition Campaign NIF had about 36 different types of diagnostics. These were based on several decades of development on Nova and OMEGA and involved the whole US ICF community. A plan for a limited of NIF Diagnostics was documented by the Joint Central Diagnostic Team in the NIF Conceptual Design Report in 1994. These diagnostics and many more were installed diagnostics by two decades later. We give a short description of each of the 36 different types of NIC diagnostics grouped by the function of the diagnostics, namely target drive, target response and target assembly, stagnation and burn. A comparison of NIF diagnostics with the Nova diagnostics shows that the NIF diagnostic capability is broadly equivalent to that of Nova's in 1999. NIF diagnostics have a much greater degree of automation and rigor than Nova's and the NIF diagnostic suite incorporates some scientific innovation compared to Nova and OMEGA namely one much higher speed x-ray imager. Directions for future NIF diagnostics are discussed.

1 The (long) history of the NIF Diagnostics.

Community experience in the measurement of high energy density plasmas has been accumulated over several decades on large laser and pulsed power facilities as well as at the Nevada Test Site. The scientific progress has been discussed at the biennial series of High Temperature Plasma Diagnostic (HTPD) Conferences which started in the seventies. HTPD had its 20th meeting in 2014 in Atlanta. As usual the conference it is comprehensively documented in special volumes of the Review of Scientific Instruments.

Large High Energy Density experimental facilities such as NIF, OMEGA and Z, have evolved since the early seventies. In parallel with the machines the diagnostic technology has also evolved as has the ability to routinely operate these diagnostics. Facility users are often not aware of the details of the diagnostics and as a result it is important that they can be operated reliably and accurately with routine data analysis and archiving. At LLNL experience of operating a suite of diagnostics on a large laser system for users was accumulated on the Nova laser (1) which operated from 1984 to 1999 and eventually had about 100 diagnostic systems. In parallel with Nova., OMEGA at LLE in various incarnations, and pulsed power machines at SNL have also matured as user facilities with the need for routine reliable and accurate diagnostics suites. The importance of operational and engineering support in diagnostic set up, and control, data recording, analyzing and archiving for the users has also evolved from an afterthought (most of the diagnostics were eliminated from the NIF Project after a few years!) to a major part of the operations of the facility.

Plans for NIF diagnostics began with the Nova Technical Contract (NTC) in the early 1990s which demonstrated at Nova scale the important parameters (such as plasma scale length and implosion convergence) needed for ignition. The scope of the NIC diagnostic set evolved with as the diagnostics needed for the NTC, ~1/3 scale NIC, were refined. At that time, the Joint Central Diagnostic Team (JCDT) was formed with members from all of the US ICF sites to coordinate efforts. Working with their home laboratories the JCDT developed plans for NIF diagnostics through ICF program funding at the various ICF laboratories. Commitment from the sites was largely based on the zeal of individual scientific experts in particular diagnostic disciplines at the different sites. The resulting strategy called for a national effort to develop and implement a comprehensive suite of diagnostics on NIF to be implemented in a phased manner. There was some planned duplication where multiple diagnostics would be available to measure key observables of the experiments. The need for multiple complementary diagnostics was recognized as an essential requirement because no single diagnostic makes a perfect measurement.

The Nova experience as well as experience from the OMEGA laser and the pre Z facilities provided the scientific and engineering basis for the JCDT to plan for the initial set of Diagnostics on the NIF. The mission of the ignition program drove the measurement requirements and thus the plans for the initial diagnostic set. The first documentation of the proposed NIF diagnostics was in the NIF Conceptual Design Report (2). The CDR defined the scope and the initial costing of the NIF project. One part of the initial NIF project included target diagnostics. In the CDR the initial set of target diagnostics was defined as those required to make measurements to verify laser performance, and to perform the initial ICF target experiments of measuring the drive and symmetry of the hohlraums and to measure thermo-nuclear yield. The phase I diagnostics in the CDR are shown in table I. Table I also shows the early commitment

from LANL and SNL to support the NIF at LLNL. As NIF evolved over the two decades from the CDR to NIC completion, the national involvement broadened to also include LLE, GA and MIT and NSTech. AWE and CEA were also involved.

Diagnostic	Acronym	Lab	Specs	Nova equivalent
Laser validation-pointing, focusing, and synchronization				
Static x-ray imager (ruggedized)	SXI	LLNL	20 μm , Wolther, axial view	KB
Streak x-ray cameras	SSC	LLNL	5 ps, 50 μm , 2–5 cm field	SSC
Twelve-inch manipulator	TIM	LLNL	Universal vacuum load-lock manipulator system	SIM
Hohlraum temperature tuning and shock timing				
Soft x-ray power diagnostic	SXSS	SNL/LLNL	time-resolved broadband x-ray spectrometer	SOP
Shock break out systems	SOP	LLNL/SNL	time-resolved $f/10$, uv microscope active and passive	SOP
Filter fluorescer	FFLEX	LLNL	high-energy x ray and spectrum 5–300 keV	FFLEX
Hohlraum symmetry tuning				
Gated x-ray imaging system	GXI	LANL/SNL	80 ps, 5–10 μm 2–10 keV x-ray imager	GXI
Target yield	YN	SNL	10^7 – 5×10^{20} activation (In,Cu)	Yield
Neutron time of flight	NTOF	LANL	10^8 – 10^{15} current mode GCNTOP	
Neutron imaging	NI	LLNL	10 μm , 10^{12} DT, 10 cm TIM, $M =$	NPAM
Soft x-ray imager	SXRI	SNL	30 μm , 300 ps, normal incident multilayer at 250 eV normal incident	GSXRFC

Table I: the NIF Diagnostics in the NIF Conceptual Design Report in 1994.

There was a period of 20 years between the CDR and the completion of NIC but most of the CDR diagnostics were implemented as described below where the nine NIF CDR diagnostic types from 1993 are compared with actuality (italicized) in 2013.

CDR_ Streaked slit camera (SSC). Two x-ray streak cameras were to be fielded in close proximity to a target using the first pair of TIMs. These cameras were to provide time-resolved x-ray images and/or spectra with spatial resolution of about 50 micron, similar to the ones on Nova. A pair of the cameras was planned for beam synchronization activities. On NIC the original x-ray streak cameras were replaced by DIM Insertable Streak Cameras (DISC) (section 3B).

CDR_ Static x-ray imager (SXI). The static x-ray imagers were to be x-ray microscopes providing time-integrated images at 2.5-keV photon energy with 25 micron spatial resolution. They were to have a 1-cm field-of-view from close to the poles of the target chamber so that x-ray images of the hohlraum laser entrance holes can be taken routinely. Together with the gated x-ray imagers, these diagnostics were to be required for the beam smoothing implementation and beam pointing and spot-size measurements. *On NIC these became the two SXI instruments (section 3A).*

CDR-Time-resolved x-ray imagers (GXI). Time resolved x-ray imagers were to provide time-gated x-ray images at photon energies between 2 to 10 keV with a temporal resolution of 30 ps and a spatial resolution of 5 to 10 micron. These were to be used primarily for hohlraum symmetry tuning. Because they will be based on x-ray pinhole technology, they were to be fielded in the TIMs. *On NIC these became the GXD and hGXI detectors(section 3B) and they were fielded in the DIMs..*

CDR_ Soft x-ray power diagnostics. The time history of the hohlraum radiation temperature was

to be measured by two techniques that were successfully used on Nova. The x-ray flux escaping from a small hole in the hohlraum wall was to be measured by an absolutely calibrated, broad band, time-resolving x-ray spectrometer. This instrument was to be either similar to the Nova Dante system or to use a new technique presently being tested on Saturn at Sandia National Laboratory, Albuquerque. *On NIC these became the two DANTE detectors(section 3A).*

CDR Soft x-ray imager (SXR1) The soft x-ray imager was to record low energy, gated x-ray images used to measure beam pointing and spot size and hohlraum symmetry. *On NIC this became a soft x-ray snout.*

CDR High energy x-ray spectrometer (FFLEX). The high energy x-ray spectrometer, similar to the FFLEX diagnostic on Nova, was to be an absolutely calibrated filter fluorescer array used to measure the photon spectrum in various energy channels from 5 keV to 100 keV. *On NIC these became the FFLEX(section 3A)*

CDR-Shock break-out diagnostic (SOP). The shock break-out diagnostic was to be similar to the streaked optical pyrometer (SOP) on Nova. It was to provide a time-resolved measurement of the optical signal created by the shock breakout from the target. In addition to the passive system used on Nova, an active version of this system was to be designed to enable measurements over wider dynamic range in radiation temperature. This system will measure the time-resolved loss in reflectivity of a probe laser beam on a witness plate, thereby determining hohlraum radiation temperature history. *On NIC this became the SOP. The active detector became the VISAR (section 3B) .*

CDR-Total neutron yield (Y) detector. The total neutron yield was to be determined by measuring the neutron activation of various detector materials. *On NIC these became the NAD detectors. (section 3C.1).*

CDR-Neutron time-of-flight (nToF) detector. A scintillator based neutron time-of-flight (nTOF) detector was combined into one detector with the functions of Nova's Large Area Neutron Scattering Array (LANSA) and the Nova ion temperature diagnostic. It was to require a collimator near the target chamber. The 10 m diameter spherical clear space that is required around the spectrometer was included in the building layout in what became known as the neutron alcove. *On NIC these became the SPECE and SPEC A nToF detectors (section 3C.2).*

2 Summary of Diagnostics under NIC

2A Scientific Responsibility for NIF Diagnostics

There was nearly two decades for diagnostic innovation on Nova, OMEGA and Z between the 1994 CDR and the end of NIC. In 1997 most of the CDR diagnostics were removed from the scope of the NIF project. Responsibility for scientific development remained with the sites of the ICF program and responsibility for installation and interfacing with the facility transitioned to the LLNL ICF program. A few NIF diagnostics were installed on an early version of NIF called NEL in 2003/2004 but the installation of most of the NIC diagnostics was between ~2008 and 2013. There were many additions to the list of initial NIF diagnostics some of which are summarized in review papers (3) (4) (5) (6).

The NIC Execution Plan (EP) was first submitted to NNSA in 2006. It defined a set of diagnostics as part of the baseline configuration for NIF. The completion criteria were based on the concept of providing the diagnostics to support the experimental campaigns used to verify laser performance and measure target performance as an integral part of the experimental campaigns. The scope of the set of diagnostics was to provide a core set of radiographic, optical, x-ray and neutron diagnostics sufficient to support ignition, High Energy Density Science program and other user applications during routine facility operations.

The diagnostics in the NIC EP were similar to those on the NIF CDR: SXI(2), NBI(2), SXD(2), GXD(2), FXI(2), Dante(2), Protex, NToF, VISAR/PSBO, gamma bang time, neutron imaging, FABS 31B/36B, HEXRI, ARC, MRS, Carbon-12 activation, snouts. In fact as detailed in section 3 below all but Protex, FXI, ARC and Carbon-12 activations were implemented by the end of NIC.

In addition starting about 2007 a robust NIF diagnostic activity started. The JCDT stopped functioning about 2000 but the need for the diagnostic development to keep pace with the completion of the NIF project and the goals of the NIC EP drove a series of NIF User workshops encouraging full national support of the NIF Diagnostics. NIC Diagnostic workshops with attendances of 60-100 were started in early 2009 and were held about twice a year. The outreach process was very successful. By the end of the NIC in 2013 there were 36 different types of diagnostics, (about 65 different diagnostics in total) under full facility control. There was major external scientific responsibility for these diagnostics, LANL, SNL, LLE, MIT and General Atomics were scientifically responsible for about half of the diagnostics as discussed in section 3. Also NSTech has a major responsibility for diagnostic calibrations.

2B Engineering and Operations of the NIF Diagnostics

Because the NIF is a major user facility any new diagnostics must be interfaced to the facility and must be controlled and operated by the facility. The NIF facility provides the systems in the target area necessary for executing experiments. This includes integration, qualification, control, and operation of diagnostics, as well as the target area systems necessary for executing experiments and the requisite off-line and on-line testing and calibration.

Although all diagnostics are integrated and operated by the NIF operations and engineering staff, the responsibility for the design, construction, initial testing and accuracy of the diagnostics systems is shared among the NIC partners. The extraordinary contributions to NIF diagnostics by NIC partners and collaborators are described in the detailed descriptions of the diagnostics below, and the references at the end of this paper.

The Magnetic Recoil Spectrometer (MRS) of Section 3C below is a good example of shared responsibility. MIT developed the concept of the MRS and working with LLE installed and tested the first MRS on OMEGA. The scientific group responsible for NIF set specifications for a NIF version of the MRS. The ICF program at LLE assumed responsibility for design and fabrication of the NIF MRS at LLE. MIT, LLE, and LLNL prepared the interfacing and alignment processes on NIF and set up the data processing capability at LLNL. The instrument (see figure 12) was delivered to NIF in 2009. LLNL has formal ES&H responsibility, it operates the instrument collects the data, and etches the set of plastic (CR39) foils which contain

the data. However MIT remains to this day responsible for the operations processes, the data analysis and inputs the processed data into the NIF data archives.

LLNL is responsible for the major effort of operating the diagnostics. Operation of the set of diagnostics requires set up and control of 13,000 parameters and 1,000 control points and configuration control of thousands of diagnostic parameters. There are about 60 major data analysis algorithms. Most data is archived and is available to and searchable by qualified users. The NIF diagnostic control and data acquisition system is discussed in section 5 below.

2C The Diagnostic Manipulators on the NIF

The diversity of experimental requirements and limited diagnostic lines of sight has necessitated many of the instruments at major ICF facilities to be removable so that they can be installed in different port locations to support the varied user experimental configurations. This is accomplished with vacuum-interlocked Diagnostic Insertion Manipulators (DIMs) that are used to place and align instruments close to the target. A common manipulator policy was developed within the ICF program, starting in the 1990s. The standardized interface on TIMs and DIMs has allowed movable DIM-based diagnostics to be easily tested at or borrowed from OMEGA

The DIM is an inserter and manipulator of diagnostics into the target chamber. A vacuum interlock is provided to make it possible to withdraw a diagnostic from the chamber and work on it without disrupting the chamber vacuum. The concept is based on the very successful six-inch manipulators (SIMs) used on Nova and the ten inch manipulators (TIMs) used on OMEGA (which has six of them). The French laser LMJ in Bordeaux uses the same concept with their System for Insertable Diagnostics (SIDs). The Trident laser at LANL uses a version of the TIM.

In the CDR the NIF diagnostic manipulators were envisaged as being TIMs but during the design process the bore was increased from the nominal ten inches to about 30 cm. The DIMs are mounted to 46 cm ports on NIF with a gimbal, and supported at the outboard end by positioner, which have motorized stages. Transverse alignment of the diagnostic in the DIM is achieved by these external positioners which cause the diagnostic at the other end to pivot about the gimbal mount. The DIM is connected to the target area roughing system to pump the loading part of the DIM external to the target chamber. When the DIM is roughed down, the vacuum gate valve at the chamber port can be opened. High-vacuum pumping is done through the target chamber. The load lock of a DIM is shown in Figure 1.

For the duration of the NIC NIF had three DIMs, two in the equatorial plane at (90, 78) and (90, 315) and one polar DIM at (0,0) where the number in parentheses are the theta and phi spherical coordinates in degrees. There is a user demand for several more DIMs to be installed and plans to install two more about 2016.



Figure 1. The load-lock part of a DIM on the NIF. The outside of the target chamber is the blue surface on the left. The diagonal struts at the end of the tube are the positioner which move the outer end of the DIM which pivots on the gimbal seen just outside the chamber wall.

3 Categorization and function of NIC Diagnostics.

At the end of the NIC, NIF was equipped with approximately 60 optical, x-ray and nuclear diagnostics that together provide 300 channels for experimental data. Approximately half of the diagnostics are fielded on most shots.

It is customary to categorize and discuss the diagnostics on laser or pulsed power systems by their discipline as optical, x-ray or nuclear as is done in references (3-5). A more insightful categorization is by their principal use during the three major phases of an implosion or a planar experiment. First laser (or pulse power) energy is absorbed to create a drive usually by shock waves, that is then applied to implode a spherical or cylindrical target or accelerate a planar target. Then the target responds to the drive (e. g. the implosion) and there is target motion or shock breakout. Finally for an implosion the fuel assembles close to the center of the target. The convergence causes heating and with deuterium, tritium or helium 3 fuel, there can be

thermonuclear burn. In this major section of the paper we categorize and discuss the NIF diagnostics in these three groupings namely:

- 3A diagnostics of laser absorption and hohlraum conditions, also referred to as drive diagnostics.
- 3B diagnostics of the shock and implosion phase, also referred to as target response/implosion diagnostics because not all experiments are implosions.
- 3C diagnostics of fuel assembly, stagnation, and burn.

3A Diagnostics of Laser Absorption and Hohlraum Conditions

The NIF diagnostics that measure the laser absorption and hohlraum conditions (specifically, the radiation drive) are shown in Table II. In this and through table VI the scientific responsibility is shown, the observable as well as the acronym and a reference(s).

Acronym	Diagnostic	Contributors	Observable	Ref.
FABS31 FABS36	Full Aperture Backscatter Station	LLNL	Backscattered light into lenses	7
NBI23.5 NBI31 NBI36	Near Backscatter Imager	LLNL	Backscattered light near lenses	7
Dante1 Dante2	Broad-band, time-resolved x-ray spectrometer	LLNL	Hohlraum x-ray conditions	8
FFLEX FFLEX TR	Filter Fluorescer	LLNL/AWE	Hot electron fraction and temperature	9,10
SXI-L SXI-U	Static X-ray Imager	LLNL	Laser entrance hole size and beam pointing	11, 12
EHXI	Equatorial Hard X-ray Imager	LLNL	Beam pointing in the hohlraum	
EMP	Electromagnetic Power	LLNL	Microwave generation	

Table II Diagnostics of laser absorption and hohlraum conditions.

FABS and NBI: The energy that is absorbed by the target is the input laser energy minus the light that leaves the target. For coherent light sources, most of the light leaving the target is back or forward scattered by stimulated Brillouin or Raman scattering. For x-ray drive targets, most of the laser energy that is not absorbed comes back into or close to the focusing lenses which are arranged in sets of four on NIF. The light backscattered into the lenses has a small transmission through the final turning mirror (which are 1ω mirrors) and is measured by the Full Aperture Backscatter Stations (FABS) on two representative quads of the inner and outer beams (at 30 degrees and 50 degrees respectively). Streak cameras connected to spectrometers in FABS measure time and spectrally resolved stimulated Brillouin and Raman backscattering spectra SBS, SRS. These systems are called FABS30 and FABS50, respectively (7).

In addition some light is scattered in the area around the lenses and is measured by the three Near Backscatter Imager (NBI) diagnostics on representative quads, an outer quad of beams at 50 degrees, and two inner quads of beams one at 30 and the other at 23.5 degrees. The NBIs consist of scatter plates (see Figure 7) surrounding the incident beam path close to the target chamber wall and a small scatter cross near the chamber wall between the beam apertures in one quad of beams at 23.5 degrees. The intensity of light onto the scatter plates is observed from outside the target chamber through a view-port with a line-of-sight to the scatter plates..

Dante1 and Dante2: Dante1 and 2 are fixed soft x-ray power diagnostics mounted on the lower and upper hemispheres of the target chamber to see the inside of a hohlraum through its lower or upper laser entrance hole respectively. Each Dante has 18 different spectrally and time-resolved channels. The spectral ranges are determined by the filter packs, and for some channels grazing incidence metallic mirrors. The delicate and expensive filters are mounted on a filter wheel (see Figure 2) which is replaced often. The channels are centered at x-ray energies from 100eV to about 10 keV. Dante1 has five mirrored channels, and Dante 2 has eight mirrored channels.

Each channel is absolutely calibrated by measuring the diode sensitivity, mirrors reflectivity and transmission of its thin x-ray filters on a synchrotron source (8). The photo-diodes are connected by long cables to transient digitizers in electrically screened areas. As shown in Figure 2 the diodes are about 2 m outside of the NIF target chamber, 7 m from the target. Nevertheless the x-ray flux on the soft channels can cause space charge saturation of the electron emission close to the photo-cathode. This effect is mitigated by attenuating the x-rays by a fine array of holes in a disc placed at the location of the filter wheel so that the x-rays through the holes onto the photo-cathode are sufficiently diffracted onto the photo-cathode to avoid local saturation. The time resolution is approximately 150 psec after de-convolving the response function of the cables.

After spectral de-convolution Dante measures the x-ray power per steradian through a laser entrance hole (LEH). With knowledge of the size of the LEH including its closure during a laser pulse measured by the SXIs, Dante determines the time-dependent radiation temperature in the hohlraum from the Stefan-Boltzmann law.

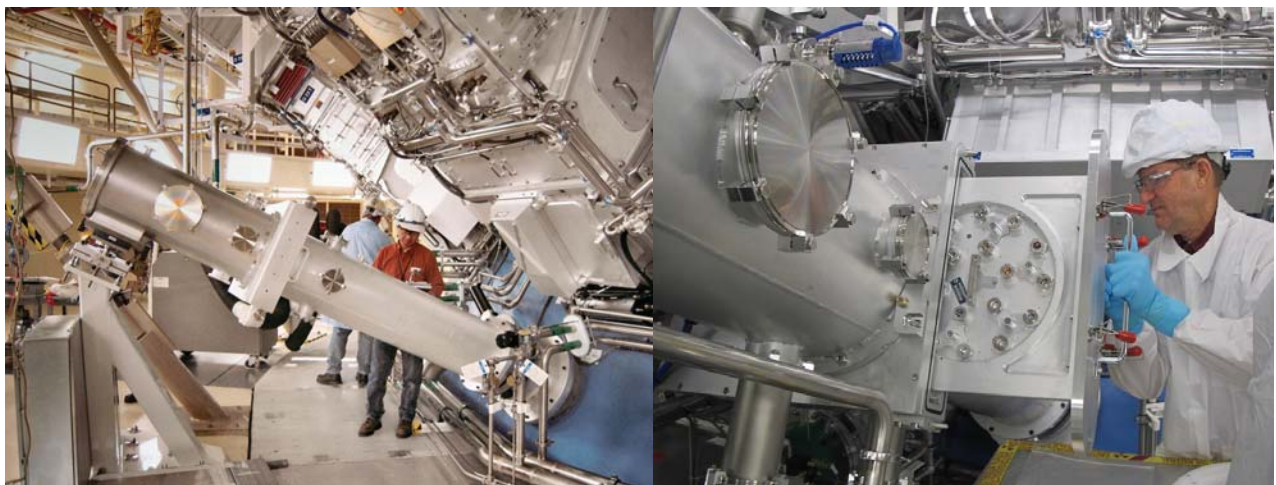


Figure 2. The upper Dante diagnostic with a close-up of the Dante filter wheel being inserted, shown at right.

FFLEX: The Filter Fluorescer (FFLEX) diagnostic measures the absolute hard x-rays energy in ten spectral bands (15 keV to 400 keV) with time resolution initially implemented on two channels (9). Figure 3 graphically illustrates the radial placement of the photo-multipliers and scintillators which

measure the light output from filtered fluorescers up to 100 keV for eight channels. The two hardest channels only have filters since no fluorescers are available >110 keV. Recently all channels were upgraded to have time resolution (10).

After de-convolution of the channels impulse response function measured using a short pulse laser system, the FFLEX time response is <400 ps. The absolute energy response of the photo-multipliers and scintillators is measured at NSTEC using a filtered fluorescer High Energy X-ray source (HEX) and absolutely calibrated detectors. The hard x-ray spectrum determines the “temperatures” and energy of hot electrons using a model of continuum x-ray emission from a spectrum of high energy electrons. These energetic electrons generated by laser-plasma instabilities (LPI) can penetrate through the capsule ablator and preheat the DT fuel, compromising fuel compression (9).

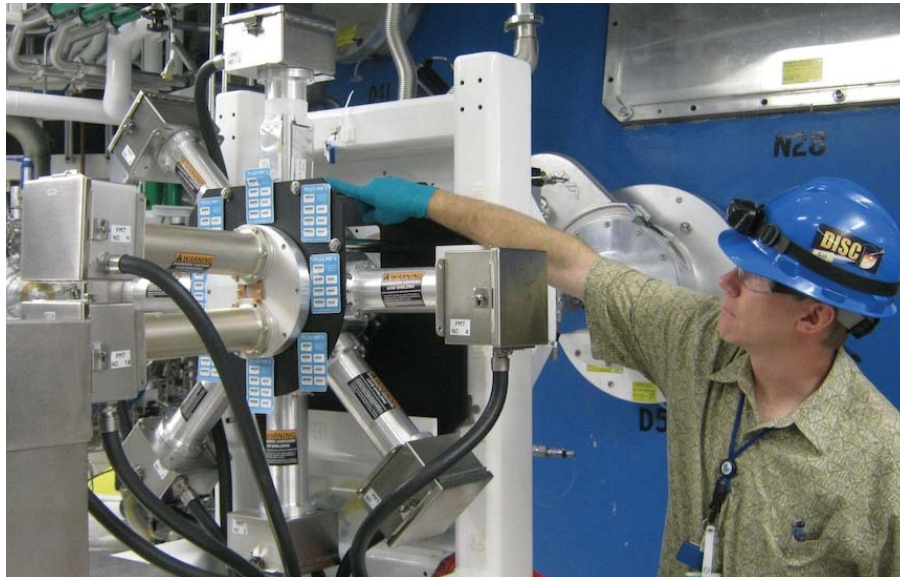


Figure 3. The FFLEX x-ray diagnostic measures the hard x-ray spectrum. Shown are the eight radial direction channels, which were time integrated at the time of the NIC, and on the left the two harder (higher energy) channels, which are time resolved.

SXI-U and SXI-L: Two Static X-ray Imager (SXI) diagnostics (upper hemisphere and lower hemisphere respectively), are mounted on retractable positioners, record multiple filtered pinhole images (11,12) of the target. On some channels, spectral selection is accomplished with filters and mirrors that provide low-resolution x-ray imaging at 900 eV. Other channels only use filters, providing 3–6 keV spectral imaging. The images are recorded on either image plates or charge coupled devices (CCDs), depending on the expected neutron yield. The locations of the SXIs were chosen to view the x-rays emitted from the inner walls of the hohlraums visible through the LEHs. This x-ray emission is used as a back-lighter to measure the size of the LEH. The image is weighted by the intensity of the hohlraum wall emission most of which comes close to the end of an ignition type pulse. The size of the LEH decreases during the pulse and so the measured LEH size is less than its original size.

SXI was also one of the original diagnostics used to assist in the verification of laser pointing during NIF commissioning. These instruments can determine the positions of the laser spots focused on a planar target by measuring the resulting x-ray emission with respect to fiducial markings on the target.

EHXI: The Equatorial Hard X-ray Imager (EHXI) incorporates a static array of pinholes that form many low-resolution, hard (>40 keV) x-ray images of hard x-rays transmitted through the hohlraum wall and thermo-mechanical package (TMP) and representative of the positions where the beams are incident inside the hohlraum. The pinhole array is outside of the chamber at about 6 m from the target with the

image plate detector another 3 m further away. The low energy cut-off is set by of the x-ray absorption in the hohlraum wall, TMP, and a thinned-out target chamber flange.

EMP: The Electromagnetic Power (EMP) diagnostic measures the electromagnetic frequency spectrum in the target chamber.

3A.1 Comments on the NIF Drive Diagnostics.

The laser absorption fraction is measured with adequate accuracy. With the NIC pulses the absorption was typically 80-85%. However several aspects of the drive in the hohlraum should be improved. The Dante spectrometers have a spectral resolution of only a few. A crystal spectrometer with spectral resolution about 100, viewing through the LEH, will improve the knowledge of the x-ray drive spectrum, particularly the fraction above 2 keV.

The LEH closes significantly during an implosion. There is a large loss of x-ray energy through the LEH and so a knowledge of its time dependence is important. The SXIs use the natural backlighting from the hohlraum and takes a time integrated, emission weighted measurement of the LEH size. Nanosecond time resolution on the SXI will directly measure rather than model the closure rate of the LEH without relying on modeling.

There are no measurements of the plasma density and temperature in the hohlraum. The spectra recorded by FABS from the SRS and SBS light depend on density and temperature but in a complex and hard to quantify manner. Optical Thomson scattering at about the fifth harmonic might enable time and spatial resolved measurements. Isoelectronic spectroscopy of tracer materials will give a measurement of state of ionization and with modeling also give an electron temperature.

3B Target Response/Implosion Diagnostics

The capsule responds to the drive and implodes(or a planar target accelerates). The x-rays produced by the interaction of the laser beams with the inside wall of a hohlraum drive pressure waves that often steepen to shocks into the capsule within the hohlraum. As a result, the capsule is accelerated inwards, causing the fuel inside to implode and after an interval of time referred to as the bang time, stagnate at the center of the shell. The capsule responds to the drive and implodes. The uniformity and velocities of the shocks, the implosion velocity of the shell, the deviations from sphericity of the in-flight shell, the shape of the hot spot at stagnation, and the interval of time when stagnation occurs are measured with the set of diagnostics shown in Table 3 which are categorized as response or implosion diagnostics.

Acronym	Diagnostic	Contributors	Observable	Ref.
SOP	Streaked Optical Pyrometer	LLNL	Shock break out	13,14
VISAR	Velocity Interferometer System for Any Reflector	LLNL/LLE	Shock velocity vs. time	13,14
DISC (3*)	DIM Insertable Streak Camera	LLNL/LLE	Implosion velocity and ablator thickness	15,16
GXD (2*)	Time-Gated X-ray Detector	LLNL/LANL	Drive symmetry for low-yield shots	17,18
hGXI (2*)	Hardened (gated) X-ray Imager	LLNL/LLE	Drive symmetry for yield <math> < 10^{15}</math> neutrons	19-21

Acronym	Diagnostic	Contributors	Observable	Ref.
NToF4BT	Neutron Time-of-Flight bang time at 4 m	LLE/LLNL	Neutron bang time	22
pToF	Proton(particle) Time-of-Flight Proton Detector	MIT/LLNL	D ³ He-proton, DD-neutron & DT-neutron bang-time	23,24
SPBT	South Pole Bang Time	LLE/LLNL	Time of x-ray emission from the imploded capsule	25
SPIDER	Streaked Polar Instrumentation for	SNL/LLNL	X-ray burn history from implosion	26
GRH	Time and spectrally-resolved Gamma Reaction History	LANL/LLNL	Gamma spectrum and time history	27,28

Table III. Target Response/Implosion Diagnostics. *In parentheses are the number of units

VISAR and SOP: The x-ray drive onto a capsule or a planar target mounted on the side of a hohlraum, produces a series of shocks, which for ignition needs to be delivered to the capsule at precise instants in time. An $f/3$ lens is held in the DIM at (90,315) to image the optical emission onto an optical streak camera. The break out time of an optically-emitting shock is measured with the Streaked Optical Pyrometer (SOP). An SOP was used extensively on Nova.

The same $f/3$ lens is also used for the Velocity Interferometer for Any Reflector (VISAR). The progress of the shocks through an optically transparent material (ablator or ice) is measured by the reflection of a probe laser beam off the shock wave into the VISAR (Figure 4). The Doppler shift of the reflected light is measured by a Mach-Zehnder interferometer to obtain the time history of the velocity of the reflecting shock to high accuracies. The VISAR technique as used on a laser facility was developed extensively on OMEGA in the early 2000s (13,14). VISAR has been very successfully used for shock timing up to the beginning of the fourth shock. A variant of VISAR technique uses a tiny mirror mounted inside a capsule that allows viewing the inside wall of the capsule at two different positions simultaneously. This is referred to as the dual-axis VISAR technique.

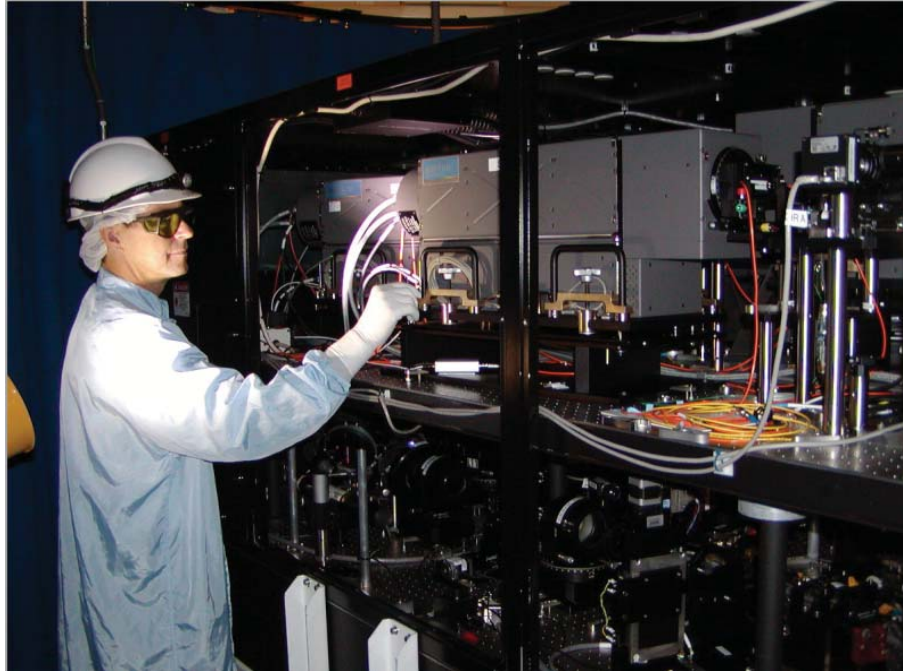


Figure 4. Technician is shown aligning VISAR, an interferometer used to measure shock timing.

DISC: The trajectory (radius versus time for spherical targets, or position versus time for a planar experiment) of the imploding shell is measured with DIM Insertable x-ray Streak Cameras (DISC). These are x-ray streak cameras that have been designed to function in the harsh electromagnetic environment of the NIF target chamber(15),(16). Imaging is achieved by mounting a space-resolving slit orthogonal to the time resolving slit of the streak camera with varying spatial magnifications up to about 10. A bright uniform source of x-rays is placed behind the imploding target and the position versus time of the shell measured by the absorption of the backlighting x-rays by the target. An earlier version of the x-ray streak cameras established the initial beam synchronicity of arrival time at target chamber center (TCC)(15). The x-ray streak cameras are used mainly to measure the position and width of the shell as a function of time using x-ray back-lighting (17). To monitor the fidelity of the streak rate and the timing, an ultraviolet 4ω fiducial (ultraviolet light) can be displayed on the edge of the streak record (18).

GXD and hGXI: When the imploded shell converges at its center, it heats, stagnates, and emits x-rays. The shape and time history of the x-ray emission depends in a complex way on the velocity and symmetry of the implosion and thus the intensity and symmetry of the x-ray drive. Following the evolution of the shape of the hot spot and drive symmetry by x-ray imaging is a technique that has been widely used in the ICF program for several decades (19). The GXD instrument uses an array of pinholes projecting many images onto an electrically gated micro-channel plate (MCP). On one MCP measurements are made at several times by coating several (typically four) strips across the MCP. Typically, the active area of these detectors is located about 1 m from TCC with the array of pinholes as close as 8 cm from the target. The array of hundreds of pinholes is laser drilled to a diameter of about 10 micron in a 60 micron thick Ta disc which is usually replaced every shot. Using an array of pinholes relaxes the alignment tolerance of the instrument to many hundred microns.

Gated X-ray Detectors (GXDs) have evolved over many years to be sophisticated instruments with many control points (16). The instruments called GXDs (gated x-ray detectors) use CCD detectors behind the gated MCPs and phosphors (Figure 5). Data from the CCD is available immediately after a shot but because of neutron induced noise on the CCD their use is limited to yield environments up to about 10^{13} 14.1 MeV neutrons per shot. To use gated x-ray imaging at a higher yield (up to about 10^{16} neutrons), hardened Gated X-ray Imager (hGXIs) are used (20). In these, the CCDs are replaced by optical film,

which is less sensitive to neutrons. Recent post NIC work has examined subtle features of these gated instruments such a gain droop and cross channel coupling effects which arise because different coated strips on the MCP are close to one another (21).



Figure 5 Hardened Gated X-ray Imager (hGXI) with imaging snout attached. The hGXI is the rectangular box at the back. The pinhole assembly at the front (left) end of the snout is typically located 8–10 cm from the target.

NTOF4BT: When the imploding target stagnates and heats, thermonuclear neutrons can be emitted for 100 to 200 psec, a short time compared to the implosion or run-in time of several nanoseconds. A neutron detector that is relatively close to TCC can measure the time at which the burn or bang occurs. Measuring this time interval or the bang time (BT) helps to constrain the radiation drive. The Neutron Time-of-Flight-4BT (nToF) detector (22) is housed in a short re-entrant well in the target chamber 4 m from the target and measures the emission or bang time of neutrons. This detector uses a diamond radiation induced conductivity (RICs) detector and is close coupled to a transient digitizer.

pTOF: Some implosions on NIF have a gas fill of pure deuterium (D) or deuterium and helium-3 (^3He), producing 2.45 MeV neutrons from the D-D fusion reaction and 14.7 MeV protons from the D- ^3He fusion reaction. The time of peak fusion production for these reactions (“bang-time”) is measured with the particle Time-of-Flight (pTOF) proton detector (23) as shown on Figure 6. As with the nTOF4BT the detector uses the radiation (particle) induced conductivity in a synthetic diamond wafer detector.

As the pTOF is positioned on a DIM the signal is recorded through ~ 150 feet of cable onto a transient digitizer. The bang-time is determined by forward-fitting a Doppler-broadened particle source function convolved with the measured instrument response to the data. This technology has been extensively developed with direct-drive implosions on OMEGA, and has demonstrated agreement with other NIF bang-time diagnostics on over 40 DT-neutron-producing implosions. Due to its fielding position 50 cm from the target chamber center, pTOF is the only NIF diagnostic capable of measuring bang-time using the lower-energy DD-neutrons, and has measured bang-times using neutron yields as low as 3×10^{10} . The sensitivity and proximity of pTOF have allowed it to also provide both DT- and TT-neutron bang-time measurements on hydrodynamic mix experiments and the DD-neutron bang-time measurement on a collision-less shock experiment.

For D ^3He -filled x-ray driven implosions, the peak areal density is high enough that the 14.7 MeV D ^3He -protons produced during the main period of fusion reactivity (‘compression-bang’) do not escape the implosion. However, the rebounding shock prior to peak compression generates a period of fusion reactivity near the time of peak implosion velocity (‘shock-bang’), when the areal density is low enough for protons to escape. If hard x-ray backgrounds are sufficiently low, the pTOF shielding is reduced so that these protons can be measured. The pTOF has measured the shock-bang time using D ^3He -protons

and the compression-bang time using DD-neutrons on a recent near-vacuum hohlraum implosion with low x-ray background. This bang-time differential is an important forensic for the shock-dynamics and hotspot adiabat of ICF implosions. In combination with WRF-measured areal density at shock-bang time, the measured shock-bang time will provide an important constraint on models of implosion dynamics.

To obtain a measurement of shock- and compression-bang time from gas-filled hohlraum implosions with large hard x-ray backgrounds, an upgraded system (MagPTOF) will use a permanent magnet to deflect D^3He -protons around substantial x-ray shielding, improving the signal to background by three orders of magnitude (24).



Figure 6. The particle-time-of-flight (pTOF) detector is mounted on the side of the x-ray imaging snout. Here a technician assembles a snout supporting three Solid Radiochemical Collection detectors (top left and bottom) and a pTOF detector (top right) for an experiment. PTOF determines the timing of fusion production using a diamond detector that responds to neutrons and protons. The end of the snout has a pin-hole array which is inserted on a DIM to about 10 cm from the NIF implosion. The assembly shown in this figure is attached to an air-box that has a time resolved detector such as a GXD or a DISC.

SPBT: The South Pole Bang Time (SPBT) detector measures through the lower (south) hohlraum LEH the time of peak x-ray emission (peak compression) relative to the laser pulse of the implosion (25). This interval, which is of the order of 20 nanoseconds from the start of the laser pulse for so called “low-foot” ignition implosions, is referred to as the “x-ray bang time.” The instrument has a fixed x-ray RIC detector measuring the x-rays diffracted off a highly ordered pyro-electric graphite x-ray crystal at a distance of 2 m from TCC. The Bragg angle of the crystal is set and filtered so the SPBT is sensitive to a 1 keV band of x-rays centered at 10.8 keV and x-rays reflected in second order. As well as the emission from the implosion the instrument also records the x-rays from the hohlraum which are distinguishable from the implosion by their longer characteristic timescale, and because in a well designed implosion the bang time is longer than the laser pulse. Because the signal is relayed through several tens of meters of cable to an

electrical recorder, the SPBT, like pTOF can measure the x-ray bang time to an accuracy of only about 50 psec after cable de-convolution. Because of the loss of electrical fidelity through the cable the SPBT cannot accurately measure the x-ray emission history of an implosion, the duration of which is on the order of 150 picoseconds.

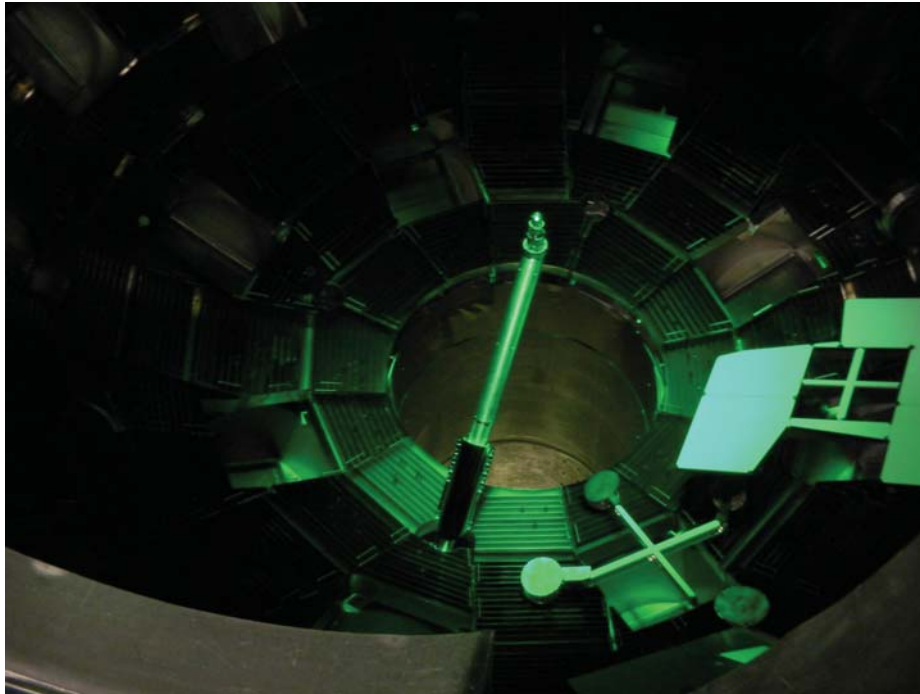


Figure 7. Viewing the lower hemisphere of the NIF target chamber. The South Pole Bang Time diagnostic is in the center on a fixed support coming in at 6:30 and is in a fixed position 2m below TCC. The scatter plates of NBI30 are on the right and the scatter cross for NBI23.5 is at the bottom right.

SPIDER: The x-ray burn history from an implosion is measured by the Streaked Polar Instrumentation for Diagnosing Energetic Radiation (SPIDER). This is a fixed instrument mounted outside the chamber (26). It measures the x-ray emission from an implosion at about 10 -15 keV through the upper LEH at a viewing angle of 7 degrees off vertical. At this angular deviation from the axis of the hohlraum the capsule is still visible through the LEH of all hohlraums used so far. The detector is a DISC x-ray streak camera, with a 4ω ultraviolet timing fiducial. This DISC x-ray streak camera is heavily shielded by polyethylene to allow the streak camera and instrument to operate up to DT neutron yields of at least 10^{17} .

GRH: The Gamma Reaction History (GRH) diagnostic measures the spectrum and time history of the emission of gamma-rays produced from the DT reaction and from gamma ray produced by neutrons interacting with matter (27). In particular neutrons interacting with carbon remaining from the ablator (28) has a bright gamma line at 4.4. MeV.

GRH is set up with four threshold spectral channels. The channel responses are typically >2.9 , >5 , >8 , and >10 MeV. In each GRH channel, gammas interact with a Be foil to produce Compton electrons, which recoil into a gas-filled cell. If the maximum velocity of the Compton electrons exceeds the speed of light in the cell adjusted by the type and pressure of the gas in the cell, they will generate a cone of broadband Cerenkov light. For each channel, Cerenkov light is relayed to a high-speed detector MCP photo-multiplier, using an off-axis parabolic mirror. This design incorporates a fixed time delay of 4.26 ns that allows the detector to recover from prompt radiation due to laser-plasma interactions from the target. The voltage signal from the photo-multiplier is used to modulate a light signal via a Mach-Zehnder and then relayed with high fidelity to a digitizer. Figure 8 shows the GRH mounted on the outside of the NIF target chamber.

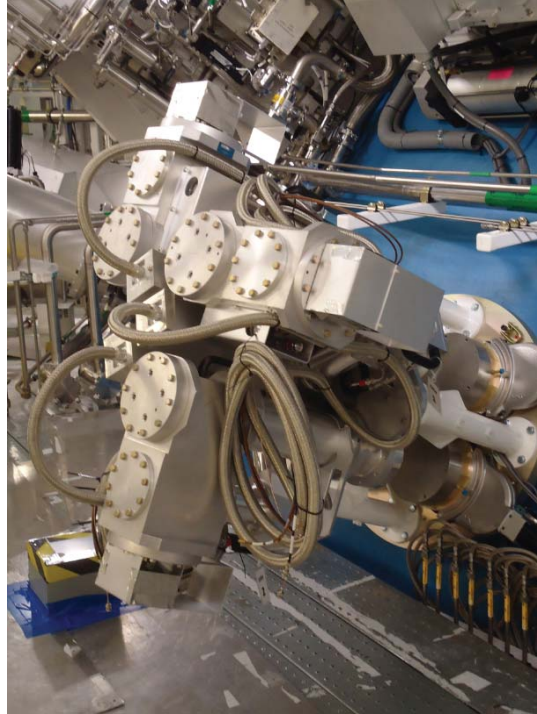


Figure 8. The Gamma Reaction History diagnostic is used to measure the time history gamma-ray emission. The four Cerenkov detectors are shown on the outside of the chamber.

3B.1 Comments on the target response diagnostics

The implosion velocity is measured by radiography onto DISC as discussed above or by radiography onto a gated camera. Implosion velocity is measured to adequate accuracy. However it is important to measure drive asymmetry. Using self emission this is measured during the stagnation phase of an implosion. To measure the drive asymmetry during an implosion requires velocity difference measurements of a few percent and this has not been possible so far.

There is planned duplication in the bang time diagnostics in this section. The SPBT diagnostic cannot measure the profile of x-ray emission because of its time response, whereas SPIDER can measure the time history of burn because it has a time resolution of about 30 psec. The neutron bang time is not necessarily the same as the x-ray time which is why NTOF4BT was built. GRH also measures the nuclear bang time but with greater accuracy. Measuring the burn profile with GRH has yet to be achieved.

3C Fuel Assembly, Stagnation, and Heating Diagnostics

As the imploding fuel and remaining ablator approach the center of the capsule, they cause the pressure and temperature of the material at the center to rise forming a hot spot at temperatures of typically many keV. This increase in pressure and temperature leads to deceleration and stagnation of the shell or ablator as well as the deuterium-tritium fuel. Thermonuclear fusion reactions that produce high-energy neutrons, gammas, and α -particles occur in the hot spot. NIF has a set of diagnostics to measure this phase of the implosion. The main attributes measured in this phase are categorized as being associated with the (1) the hot spot (yield, hot spot size and

shape, hot spot burn history, and hot spot electron and ion temperatures) section 3C.1, (2) diagnostics of the cold compressed fuel areal density section 3C.2, and (3) diagnostics of mix of the higher density ablator into the hot spot, section 3c.3. The suites of fuel assembly, stagnation, and heating diagnostics are shown in Tables 4 through 6.

3C.1Diagnostics of the Hot Spot

Acronym	Diagnostic	Contributors	Observable	Ref.
NAD—Cu	Neutron Activation Detector using Cu	SNL	Un-scattered neutron yield from a DT-filled capsule	29
NAD—Zr in well	Neutron Activation Detector (well-mounted)	LLNL	Un-scattered neutron yield from a DT-filled capsule	30
NAD—Snout indium (In)	Neutron Activation Detector (DIM mounted)	LLNL	Un-scattered neutron yield from a DD-filled capsule	31
ARIANE	Active Readout in a Neutron Environment (Gated x-ray imager)	LLNL	X-ray hot spot size and shape for yields $<10^{16}$ neutrons	32
DIXI	Dilation Imager for X-rays at Ignition	GA/LLNL	X-ray hot spot size and shape with an x-ray gate time ~ 10 psec	33
NIS	Neutron Imaging System	LANL/LLNL	Hot spot size and fuel asymmetry	34-36
NITOF	Neutron Imaging Time-of-Flight	LANL	Ion temperature	
NTOF20 IgnHi	Neutron Time-of-Flight	LLE/LLNL	Ion temperature	37
NTOF4 (3)	Neutron Time of flight 4m	LLE/LLNL	Ion Temperature, yield	

Table IV. Diagnostics of the hot spot.

The neutron yield is a primary metric of the properties of the hot spot. For 14.1 MeV DT neutrons, yield is measured by three independent absolute diagnostics namely two types of Nuclear Activation Detectors (NADs), and the Magnetic Recoil Spectrometer (MRS). These techniques are absolute in the sense that they depend on the known geometry and two different nuclear activation cross sections (copper and zirconium) and the neutron-proton or neutron-deuteron knock-on cross sections for the MRS. Cu and Zr are chosen as NAD materials because they have activation thresholds at 14 MeV and so down scattered neutrons will not give much signal. The levels of accuracy for all techniques are less than 10% and are only weakly dependent on yield for yields $> 10^{13}$. The fact that usually the three independent techniques agree to about 5% adds confidence to estimates of accuracy. A secondary diagnostic for neutron yield immediately after a shot is provided by the nToF detectors. These are secondary in that they are calibrated in situ against the three absolute detectors.

For deuterium (DD) and D-³He gas fills, the lower energy 2.4 MeV neutron yield is measured by neutron activation of an indium foil and/or absolute track counting in CR39 samples exposed to the neutrons. Unfortunately there is no threshold activation material for the DD neutrons so to avoid activation by scattering from the chamber the In NAD sample has to be held close (~ 50 cm) to the target as shown in

Figure 6. As this detector is brought closer to the n source activation from the source dominates activation from scattering by mass in the chamber. The threshold nature of the activation detector materials Cu and Zr for 14.1 MeV neutrons do not have this background problem as scattering reduces the n energy enough that there is no activation.

NAD—Cu: The copper Nuclear Activation Detector (NAD) measures the un-scattered neutron yield from DT-filled capsules by activating a copper foils (29). Copper (and zirconium, discussed below) have high energy thresholds for the (n,2n) so only the un-scattered neutron yield is measured. Copper foils are installed in the neutron beam in both the SpecE and SpecA lines of sight. . After the shot, foils are removed and the activation level is determined using standard nuclear coincidence counting techniques. Because of the rapid decay rate of the activated copper (one half-life is 9.7 minutes), the foil must be quickly removed and counted in a detector system housed in the neutron alcove.

NAD Well—Zr: The Well NAD in a well uses activation of a zirconium sample inserted into a short re-entrant well on the target chamber as shown in Figure 9 (31). Zirconium, like copper, is an activation threshold detector for 14.1 MeV neutrons. Since the half-life of the zirconium activation product is 3.2 days, the counting facilities in the basement of building B151 can be used to measure the level of activation.

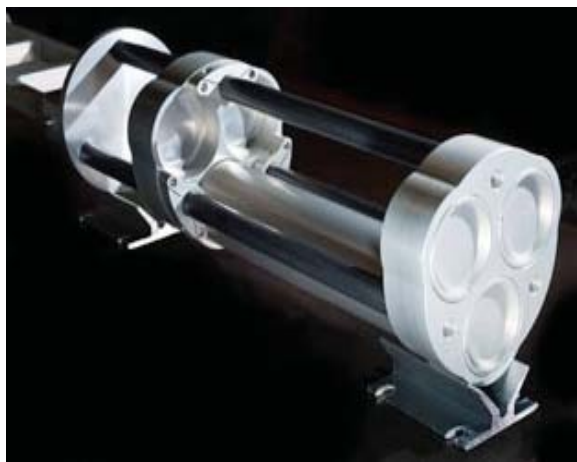


Figure 9. The Neutron Activation Detector in a well is designed to hold up to three zirconium samples at the front or back to measure un-scattered 14.1 MeV DT neutrons.

NAD—Snout: For the 2.45 MeV neutrons produced in the DD fusion reaction, indium is used as the activation detector. Because the indium $^{115}(n,n')$ activation threshold is well below the neutron birth energy of 2.45 MeV, the sample needs to be close to the TCC to decrease the fractional contribution of scattering from the chamber. Consequently, the samples are mounted on DIM snout tubes, typically on the side of gated x-ray detectors mounted within the DIMs. The half-life of the indium activation product, 4.5 hr, is comparable to the normal operational extraction time of a few hours, and so the comprehensive LLNL radiochemistry counting facilities in B151 can be also be used (31).

ARIANE: The Active Readout in a Neutron Environment (ARIANE) gated x-ray imaging detector measures the x-ray hot spot size and shape up to a yield of $\sim 10^{17}$. ARIANE uses the gated MCP technology described for GXD and hGXI but to operate in a higher neutron yield regime, the detector is moved further away to a location just outside of the target chamber (32), see Figure 10. The pinhole array is held close to the target by DIM (90,78) which is close in angle. A plan is in place to use a mirrored version of ARIANE for experiments for operation with yields in excess of 10^{17} neutrons.



Figure 10 A technician installs a film pack in the ARIANE time-resolved x-ray imager for an experiment. ARIANE uses a CCD detector to electronically capture and record x-ray data for higher-yield experiments.

DIXI: The Dilation X-ray Imager (DIXI) drifts and time dilates a photo-electron image of an implosion. The time dilation is achieved by ramping down the extraction field of the photo-electron image in a magnetic field (33). Doing this causes early photo-electrons to move away in a drift tube from later photo-electrons emitted later. A simple analogy is the ways cars spread out as they accelerate after stopping at a traffic light. The time dilation allows time resolution to better than 10 ps. This kind of time resolution is necessary because as the yield increases, the duration of x-ray emission should become less than 100 ps. At the end of NIC this instrument was just being installed on the NIF having been tested on a smaller facility but it did record NIF implosion data in 2014.

NIS: The Neutron Imaging System (NIS) creates static neutron images of the primary (14.1 MeV) un-scattered DT neutrons and the down-scattered (6–12 MeV) neutrons from a burning DT capsule. Images are formed through an array of neutron pinholes, but because of the long range of 14 MeV neutrons in all materials, the “pinholes” are precision-shaped grooves machined in 20 cm of gold plated on a tungsten substrate. Like many of NIF’s diagnostics neutron imaging was first demonstrated in the lab on Nova (34), developed on OMEGA by LANL, LLE and Commissariat Atomique Energie (CEA) staff (35) and then installed on NIF (36). The neutron pinhole array is held 20-30 cm from TCC and aligned and oriented by the DIM 90-315 manipulator when not in use for VISAR. The neutron pinhole and its debris shield are shown in Figure 11 left.

The neutron image detector system is shown in Figure 11 right. It is located 28 m from the target in a building added onto the NIF for this purpose in 2011. The detector is a coherent fiber bundle of organic scintillator (BCF-99-55) but because of the nearly mm range of the knock-on protons, a high magnification is required ($\sim 100X$) to achieve ~ 10 micron point to point source resolution. The primary un-scattered neutron image is recorded by collecting light with a lens system from the front end of the scintillator fiber array onto a micro-channel plate optical detector which can be gated for the arrival time of the 14.1 MeV neutrons. The secondary scattered image is recorded by collecting light with a fiber bundle on the back of the scintillator onto a second micro-channel plate optical detector gated for the arrival times of 6- 12 MeV neutrons. The hot spot size and fuel asymmetry are determined from the image of the primary neutrons, and the cold fuel size and shape is inferred from the down-scattered image.



Figure 11. Left: the front end of the NIS. The square object in the middle is the front end of the neutron pinhole array. The round object on the right is the debris shield in its open position to allow alignment. The other round object on the left is the converter foil for the MRS (section 3C.2). Right: the detector end of the Neutron Imaging System located 28 m from TCC. The neutrons travel from left-to-right through the detector system.

NITOF, NTOF20IgHi and nToF4 (3): There are three separate NTOF detector types whose main function is to measure ion temperature of the hot spot from the thermal broadening of the neutrons. There is another type of nToF, the spectrally resolving nToF SPECs in section 3C.2 below which also measure temperature, but whose main function is to measure areal density. The NTOF20IgHi (37) is a CVD-based synthetic diamond detector located in the neutron alcove about 20 m from TCC. The Neutron Imaging Time-of-Flight diagnostic (NITOF) is located upstream of the NIS system about 28 m from TCC. These are far enough away from the target that the “thermal” broadening is large enough compared to the instrument response function that an accurate ion temperature measurement can be made. There are three nToF4 s mounted in short reentrant well at the wall of the target chamber at a distance of about 4 m. One of then NTOF4 DD has a high sensitivity to measure DD neutron yields as low as 10^9 . Another two are NTOF4 DT lo and NTOF4 DT hi span a range of DT n yields from 10^{11} to 10^{16} . These were relatively easy to install and were used for approximate measurements of the ion temperature and over a large range of yields.

3C.1a Comments on hot spot diagnostics

Yield is adequately measured because of the different absolute techniques agree within several percentage points. As described above the detector measures un-scattered yield, including scattering from the cold fuel of the compressed target. For the layered implosion of NIC a DT areal density of ~ 1 gm/cm² was

achieved which scatters ~20% of primary neutrons. The Flange NAD array of section 3C.2 utilizes this effect.

The ability to measure the shape in presence of yield is also adequate. The principal ion temperature diagnostic are the nToF's. The set at 4m was installed early and have low resolution. The two at 20 m (section 3C.2) do not adequately sample direction. A close to south pole nToF at ~ 20m has now been fielded and plans are in place for a close to north pole nToF at ~ 20m.

3C.2 Diagnostics of Areal Density of a Compressed Target

The hot spot model of ignition envisages a high temperature low density region surrounded by a low temperature region at higher density in isobaric equilibrium with the hot spot. The areal density of compressed shell which would mainly be deuterium-tritium needs to be ~ 1.4 gm/cm² for ignition which is much higher than ever achieved in the laboratory. Techniques to measure the important areal density of the compressed target are important and are shown in table 4.

Acronym	Diagnostic	Contributors	Observable	Ref.
CR	Compton Radiography	LLNL	Fuel shape	38
MRS	Magnetic Recoil Spectrometer	MIT/LLE	n spectrum	39-42
Flange-NAD(17)	Neutron Activation Detector (Flange Mounted)	LLNL	Anisotropy of n scattering	30
NTOF20 SPEC-A NTOF20 SPEC-E	Neutron Time-of-Flight-Spectrum	LLNL/LLE	n spectrum	43,44
RAGS	Radiochemical Analysis of Gaseous Samples	LLNL	Broad band n spectrum	45
SRC	Solid Radiochemical Collection Diagnostic	LLNL/LANL	Broad band n spectrum	46
WRF	Wedged Range Filter	MIT/LLNL	Shell p energy loss for deuterium - helium-3	47,48

Table V. Diagnostics of the Areal Density

CR: Compton radiography (CR) is a measurement technique based on point-projection radiography at photon energies from 60 to 200 keV where the Compton effect is the dominant contributor to the x-ray “opacity” (of course, photons are not absorbed but scattered) The Advanced Radiographic Capability (ARC) will be a major enhancement to NIF giving it a short pulse high power capability but was not available in 2013. ARC will be used for time-resolved radiographic imaging of the dense cold fuel surrounding the hot spot by CR. Until ARC is available at NIF, CR with reduced resolution of about 30 microns is being performed using two focused 3 ω quads of NIF (38). The detector is a hardened, gated x-ray detector.

MRS: The Magnetic Recoil Spectrometer (MRS) is a fixed location neutron spectrometer that provides an accurate measurement of the compressed fuel areal density from the number and spectrum of down-scattered neutrons. An MRS was first developed on OMEGA (39). An updated version was installed on NIF in 2010 (40) as shown in Figure 12. DT neutrons interact with a plastic foil (sometimes deuterated)

held 30 cm from the target as shown in Figure 11 left, producing knock-on protons or deuterons. These charged particles are then dispersed by their momentum in a magnetic field and focused on an array of solid plastic film track detectors (CR-39) located at the focal point of the spectrometer. After a shot, the film is removed and etched and the neutron spectrum and yield are determined by the location and number of tracks on the detectors (41). The number of neutrons down-scattered in energy by the compressed DT is measured by the neutron spectrum. In addition, MRS records NIF's absolute un-scattered yield (42) and ion temperature, although ion temperature is measured with lower resolution than the nTOFs, depending on the thickness of the plastic foil.



Figure 12. The Magnetic Recoil Spectrometer is shown with four students from MIT who were key in implementing the instrument and the CR-39 detectors.

Flange-NAD: The Flange Neutron Activation Diagnostic (Flange-NAD) is unique among NIF neutron diagnostics in that it makes many simultaneous measurements of the same neutron source term from a particular shot (30). Activity induced in up to 17 zirconium pucks (“foils” as historic nomenclature) through the $Zr-90(n,2n)Zr-89$ reaction is quantified by removing the pucks and detecting the 909 keV gamma ray from $Y-89m$, the decay product of $Zr-89$. Because the 3.2 day half-life of $Zr-89$ allows for physical removal of Zr samples, the gamma spectroscopy measurement is made using lead-shielded high-purity germanium detectors in a low-background counting facility in B151. By careful design of the gamma spectroscopic measurement, the experimenter can in effect use the exact same instrument for all 17 simultaneous measurements, leaving only two major uncertainty components in the position-to-position activation ratio: the counting statistical variation and the shot-to-shot variability in the neutron source to activity transfer function. The relative uncertainty in the activation ratio between any two points can be reduced in practice to less than 2%, with the absolute DT neutron yield measurement uncertainty near 7%. The anisotropy of the un-scattered yield is measured from the variation of activation as a function of direction allowing for calibration factors. Any anisotropy in un-scattered yield indicates a variation or asymmetry in the fuel areal density. Accurately measuring the anisotropy in the neutron yield from an implosion requires an accurate cross-calibration using low areal density implosions because the compressed fuel areal density of $\sim 1 \text{ gm/cm}^2$ only down-scatters about 20% of the 14 MeV neutrons, and variations in that 20% need to be measured accurately.

NTOF20 SPEC-A and NTOF20 SPEC-E: There are two nTOFs located at a distance of approximately 20 m from TCC one in a well shielded room called the alcove (SPEC-A) and one on the equator (SPEC-E) designed primarily to measure ion temperature and down scattered neutrons. The technology for these

spectrally resolving nToF was developed on OMEGA (43). Recently the scintillator and the housing for the detectors was improved (44). The neutron lines of sight are well collimated by apertures preventing neutrons scattered off the target positioners, the DIM instruments, or the target chamber walls reaching the detectors. Consequently, these diagnostics have sufficiently low backgrounds to measure neutrons down-scattered by the fuel. These instruments complement the MRS in measuring fuel areal density. Also their location on the target chamber adds information about any anisotropy in areal density although the anisotropy in down-scattered ratio is related in a complex way to the anisotropy in areal density.



Figure 13. Neutron Time-of-Flight (top right) is shown with staff from LLE.

RAGS: The Radiochemical Analysis of Gaseous Samples (RAGS) diagnostic is used to collect and measure neutron activation products that are gaseous at room temperature (45). For example, noble gases such as krypton and xenon can be used as activation detectors by pre-loading low-levels into the ablator. The resulting krypton and/or xenon isotopes produced can be collected and chemically fractionated very efficiently by cryogenic trapping. Isotopic analysis of the collected samples, when corrected for contributions from air, can be used to obtain quantitative data on multiple capsule performance parameters such as mix of the shell material into the fuel, asymmetry of implosion, shell and fuel areal density at peak emission, and neutron yield. The apparatus is connected to the pumping system of NIF see Figure 14.



Figure 14. The Radiochemical Analysis of Gaseous Samples system collects and analyzes gases produced by NIF experiments.

SRC: The Solid Radiochemistry Collectors (SRCs) collect samples of solid target debris that contain radioactive species produced by neutron activation. For example, gold from the hohlraums can be activated by neutrons and collected as a solid sample. SRC units placed about 50 centimeters from TCC as shown in Figure 5. The SRC units are removed post-shot and the presence of radioactive isotopes is determined by radiochemical and nuclear counting techniques in B151. The ratio of gold isotopes observed in SRCs has been used to determine areal density and some measure of mix (46).

WRF: Wedged Range Filters (WRFs) are used to measure the energy spectrum of the protons from D-³He gas-filled implosions (47). The escaping thermonuclear protons primarily lose energy in the compressed ablator. When the areal density of the ablator is about 250 mg/cm² or higher, the protons are ranged out. As a result, the shock-produced protons are typically observed, while compression burn protons are ranged out. The energy spectrum of the escaping protons is measured by passing them through a wedge of material (see Figure 15), after which the position and energy of the protons are recorded on a CR-39 track detector (47). Between one and four WRF units are mounted at 50 cm from TCC on each of the polar DIM and equatorial DIM (90-78). From the energy spectrum the in-flight ablator ρR , ablator center-of-mass radius, and shock proton yield are inferred (48). The technique yields valuable data prior to the full compression of ablator. The combined polar and equatorial detectors also enable measurements of the in-flight low-mode ablator symmetry with this technique (48b).



Figure 15. The Wedged Range Filter detector unit.

3C.2 Comments on diagnostics of areal density

At the beginning of NIC it was hoped that Compton Radiography would measure the shape of the areal density of the compressed fuel, however the delay in the ARC laser has delayed the use of CR. As a result during NIC the areal density was measured by neutron down-scattering using two independent techniques of the nTOF SPEC and the MRS. The importance of areal density to ignition required two independent measurements.

The issue with using neutron down-scattering to measure areal density is that a measurement in a particular direction samples the areal density from a fraction of the shell defined by the direction of observation. For an ideal point source with an external shell some de-convolution is possible, however the accuracy of this assumption is not clear. During NIC there were three measurements of areal density along the directions of NTOF SPECA, NTOF SPECE and MRS chosen to cover reasonable anisotropy. In general the values differed by 10-20% and averages were taken. More NTOF SPECs are being planned.

Both NTOF and MRS make measurements of ion temperature and areal density which are time integrated over the implosion. Plans are being made for a time dependent MRS spectrometer to give ion temperature and areal density measurements with ~30 psec resolution during an implosion.

3C.3 Diagnostics of Mix

Acronym	Diagnostic	Contributors	Observable	Ref.
Ross Filter Pair	Ross Filter Pair	LLNL	Mix	49
Supersnout II (multi-wavelength)	Multi-wavelength X-ray Spectrometer	LLE/LLNL	Mix	50

Table VI. Diagnostics of Mix

Ross Filter Pairs: An array of “Ross filtered” pinholes records time integrated x-ray images after several different filter packs in the energy range from 8 keV to > 20 keV (49). These give measures of the temperature- and density-sensitive bremsstrahlung emission from the imploding core. This data provides estimates of hot spot mass, mix mass, and pressure, as well as broadband, time-integrated absolute x-ray self-emission images of the imploded core.

Super-snout: Two four-channel curved crystal spectrometers are used to record with medium spectral resolution the K shell x-rays from elements such as germanium or copper. These materials are added as dopants into the plastic ablaters and if the ablator mixes into the hot spot the K lines, principally He like, of the dopants emit x-rays. The intensity of the x-ray lines is an indicator of the density and temperature

of the mixed emission region (50). The spectrometer is a snout that is attached to the front of a gated detector, and the data is recorded onto image plate as shown in Figure 16. Like many other NIF diagnostics this instrument was developed and tested at OMEGA before installation on the NIF.



Figure 16. The Super-snout four-channel crystal spectrometer is attached to the recording box.

4 Locations of Diagnostics on the NIF target chamber

The locations of the target positioners (TarPos, and CryoTarPos), DIMs, and some of the diagnostic systems on the NIF target chamber are shown in Figure 17. Also shown in the Figure are FODI (Final Optics Damage Inspection system) and OPAS (Opposed Port Alignment System).

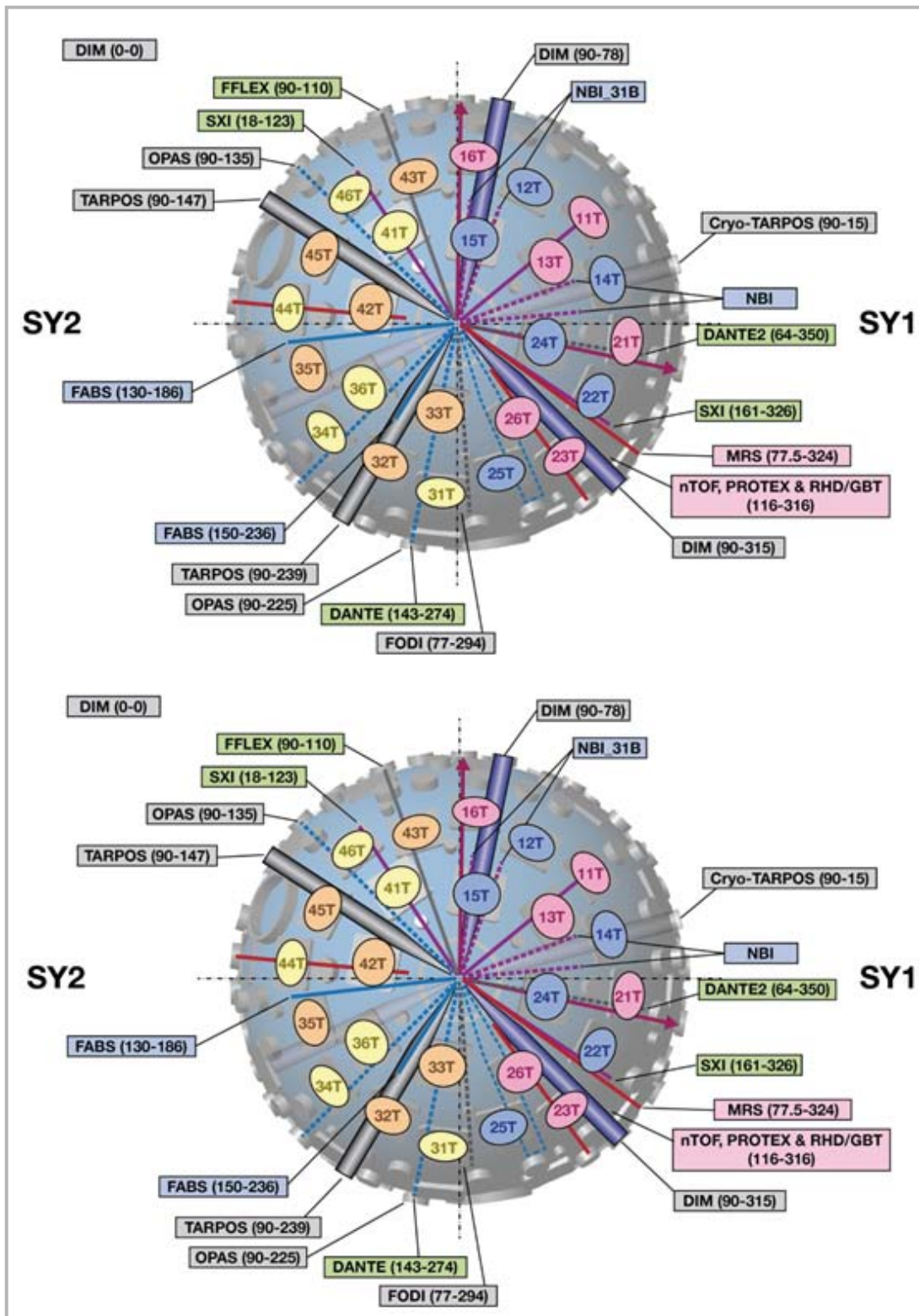


Figure 17 Top and bottom views of the NIF target chamber, showing the location of the quads and major diagnostic (Switchyards, SY1 and SY2, are shown on the right and left, respectively). NIF diagnostics are either constructed and deployed to a fixed location in the target chamber/bay or are fielded on a DIM.

5 Target Diagnostics Control System

Controls for target diagnostics are managed as part of the ICCS high-level architecture. (51) ICCS incorporates over a thousand front-end processors, servers, and workstations to control, diagnose, and fire the laser, as well as to integrate the suite of target diagnostics. Target diagnostics have unique control system requirements; they must be able to operate outside of the supervisory environment and be operated or calibrated in facilities other than NIF.

During NIC, the target diagnostics embedded control architecture was modified to use a single low-cost PC104 processor per device (e.g., a digitizer). The full diagnostic control is then composed within the supervisory software by aggregating the network-attached controllers. This approach simplifies the embedded software, improves reliability, and provides easy reuse of devices in other diagnostics.

5A Diagnostic Control System

The Diagnostic Control System (DCS) framework for NIF hardware and software was developed to:

- Reduce hardware and software costs;
- Increase efficiency by reusing software;
- Improve verification and test case coverage; and
- Speed up development turnaround for new diagnostics.

Each complex diagnostic typically uses an ensemble of electronic instruments attached to sensors, digitizers, cameras, and other devices. A diagnostic's supporting instruments (i.e., power supplies, cameras, and/or digitizers) are each maintained by a dedicated computer controller with generic DCS software customized to that instrument. Figure 18 illustrates this architecture for the Dante soft x-ray spectrometer diagnostic. The Dante diagnostic uses one DCS controller with software and interface hardware specific to the power supply and 20 more controllers with software and interface specific to the oscilloscope. The various DCS computers are located in standard 19-inch electronic racks in one of four diagnostic mezzanines adjacent to the NIF target area shielding wall, along with the power supplies and digitizers. Computers are connected to the ICCS network through network switches in the diagnostic mezzanine. These controllers are diskless and boot from a file server over the network. Experimental data collected from cameras and digitizers by each controller are sent to the file server for processing and archiving.

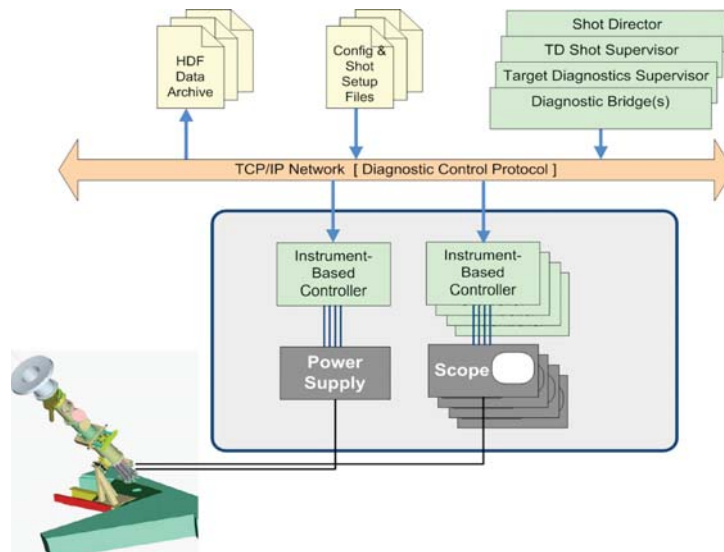


Figure 18. Diagnostic control system architecture as applied to the Dante x-ray diagnostic.

Figure 19 illustrates the DCS framework, which instantiates objects that perform the following common functions. In the DCS architecture, each instrument is interfaced to a low-cost Windows processor and JAVA application. The JAVA framework provides data management, control services, and operator GUI generation. DCS instruments are reusable by replication with reconfiguration for specific diagnostics in extensible markup language. Advantages include minimal application code, easy testing, and high reliability. Collaborators save costs by assembling diagnostics with existing DCS instruments.

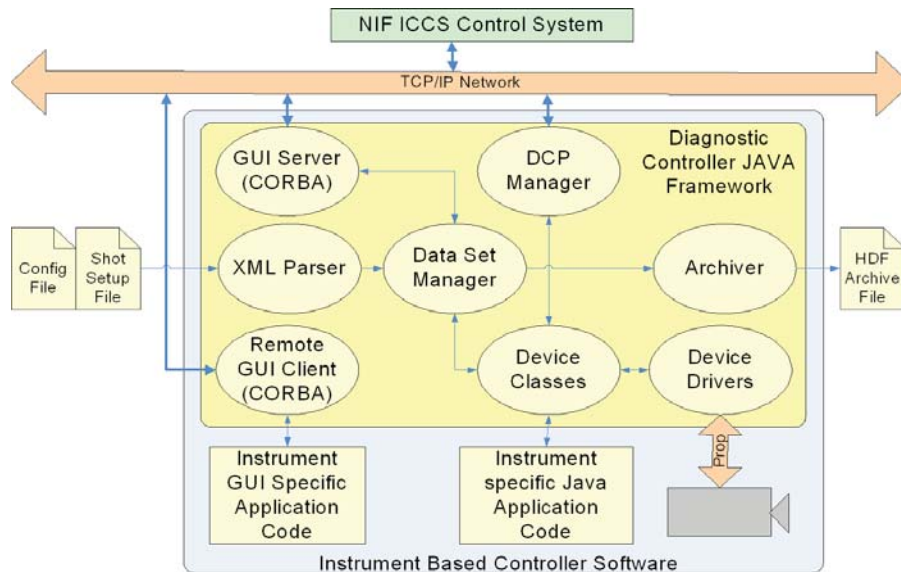


Figure 19. Diagnostic control system framework.

5.B Target Diagnostic Supervisor

The ICCS target diagnostic subsystem is a target diagnostic front-end processor containing diagnostic bridges and supervisory and shot control software. Diagnostic bridges translate DCP protocol messages from each DCS instrument into ICCS CORBA-distributed objects. The target diagnostic supervisor uses these bridges to provide status and control of each DCS instrument, and groups the set of instruments for the diagnostics they support. The target diagnostic supervisor also provides the primary operator interface at the target diagnostic console in the control room. The shot supervisor executes macro-steps that are defined in a shot model for participating diagnostics on any given shot. Instrument configuration for a specific diagnostic and shot combination is established in configuration files by the responsible diagnostic engineer. After review of the post-shot data from a given diagnostic by the responsible diagnostic engineer, it is made available to the user via the Archive Viewer (52).

6 Comparison of NIF and Nova diagnostics

It is interesting to compare the diagnostic set on Nova in the late 90's and NIF as detailed above. Nova was turned on about 1984 and so the comparison is between a teenager in the twentieth

century and a five year old now. Nova had a ten beam and a two beam chamber. The comparison here is for the ten beam chamber of Nova. The two beam chamber was mostly used for x-ray laser research and so had some very specialized soft x-ray spectrometers.

Optical diagnostics	Nova	NIF
Streaked optical pyrometer	SOP	SOP
Streaked interferometer	visar	VISAR
Streaked optical spectrometers	SOS,BSS	
Multiple streaked spectroscopy	MATRES	
Spatially discr. streaked optical spectr.	SDOSS	
Calorimeter array	EBM	
Full beam back scatter	SOS5	FABS
Near back-scatter	NBI	NBI
Thomson Scatternig	2w	

Table VII Comparison of optical spectrometers and imagers for NIF and the ten-beam chamber of Nova

NIF is missing some of the optical diagnostics that Nova had, in particular Thomson scattering to measure plasma density and temperature. Concepts are being developed to put 5w Optical Thomson scattering on NIF in a few years time to measure the density and temperature inside hohlraums. The EBMs on Nova were set up to measure scattered light at many locations. There are some discussions to make an equivalent diagnostic for NIF for direct drive but is not recognized as being of high value at the moment.

X-ray imagers	Nova	NIF
Wolther x-ray microscope	22x	
Gated x-ray pin hole camera	GXI,WAX,GACS,GSIX	GXD,hGXI
Axial pin hole cameras	APH	Polar GXD
Low resolution imagers	Kirkpatrick Baez microscopes- 8X	SXI-U&L
Neutron hardened gated imager		ARIANE, DIXI
Hard x-ray imager		EHXI
Gated soft x-ray framing camera	SXRFC	Snout
Streaked soft x-ray imager	NSDSS	Snout
Ring aperture microscope	RAM	
Streaked slit/array imager	SSC/SMP	DISC

Table VIII Comparison of x-ray imagers for NIF and the ten-beam chamber of Nova.

Nova had both KirkPatrick Baez and Wolther x-ray reflective optics. However these were designed during the planning phase of Nova before it was realized that on Nova pinhole arrays functioned well. However there are plans for a KB and in the long term a Wolther on NIF mainly

because of the need to go to harder x-ray imaging utilizing the new technology of ultra-smooth x-ray reflecting layers for hard x-rays. The ring aperture imaging on Nova allows for high spatial resolution but in practice it was rarely used. NIF does have one item of new technology and that is the drift tube technology which was installed on NIF but not demonstrated on NIF until about 2014

X-ray spectrometers	Nova	NIF
Streaked crystal spectrometers	NSCS, Keanetech 2	NXS
High resolution streaked spectrometer	HICKS	
Static crystal spectrometers	Henway,POS	
High resolution crystal spectrometers	HOPS	
Gated crystal spectrometer	TOPS	Supersnout
Gated imaging XUV spectrometer	IXUVS	
Laue spectrometer	HETS	TARDIS
Low resolution x-ray diode array	Dante	Dante
Low res. high energy fluorescers	FFLEX	FFLEX

Table IX compares x-ray spectrometers for NIF and the ten beam chamber of Nova.

NIF has been relatively slow in fielding x-ray spectrometers but is comparable to Nova in its lower resolution ($R < 1000$) capability. There are plans to build a higher resolution spectrometer for NIF in the medium term. NIF had no soft x-ray capability at the end of NIC but x-ray transmission capability has been introduced recently.

Neutron diagnostics	Nova	NIF
Yield	Cu & In NAD	Cu, Zr & In NAD
Yield anisotropy		Zr NAD-Flange
Bang time	NETMCP,GaAs	nToF4 BT
Medium res. neutron spectrometer	NTOF	nToF4, nTOFSPEC
Ultrahigh res spectrometer	fNTOF	NITOF
Burn history (n,x-ray)	NTD & GaAs	GRH, SPBT, SPIDER
Hi Res N spectrometer	LaNSA	
High res high sens spectroscopy	LANL Ti	
Neutron spectrometer		MRS
Proton spectrometer		WRF, pToF
Neutron imager	NPAM	NIS
Solid collection	SIM	SRC
Rapid collection	Rabbit	
Gaseous Collection		RAGS

Table X compares neutron and gamma diagnostics for NIF and the ten beam chamber of Nova.

The neutron diagnostic suites on Nova and NIF are broadly comparable considering the lower areal density on Nova. Nova had two high resolution single hit spectrometers LaNSA and the LANL Ti neutron spectrometer. These were used to measure the Doppler broadening of the primary neutrons and to measure the secondary DT spectrum from DD implosions. On NIF because the yield is higher the NIToF specs and the MRS accurately make these measurements and more. A single hit detector for high resolution low energy neutron spectroscopy on NIF has been discussed but there are no plans at the moment.

The neutron burn profile diagnostic on NIF was the neutron temporal detector (NTD) which uses a scintillator close to the target and an optical streak camera to differentiate the fast rising and relatively slow falling optical scintillation. This instrument then went to OMEGA. In contrast the higher yield of NIF allowed the use of the low emission rate of the 17 MeV fusion gammas using GTRH. A quantitative comparison of NTD and GRH from OMEGA is still under study.

7 Summary and Conclusion

The history of the 36 different types of NIF diagnostics was described in sections 1 highlighting the role of the whole US ICF community. A history of scientific cooperation on diagnostics is documented in the proceedings in the Review of Scientific Instruments of the long-lived High Temperature Plasma Diagnostic meeting. In making the case for the NIF, a national management team, the Joint Central Diagnostic Team, formulated the plan for NIF Diagnostics which they documented in the NIF CDR. These diagnostics proposed two decades ago were all installed on the NIF with small changes. In section 2 the NIC proposed diagnostic execution plan is described and compared with the final state of the NIC diagnostics. Section 3 is a functional description of each of the 36 different types of NIC diagnostics. The descriptions are grouped by the function of diagnostics, namely of drive in section 3A, target response section 3B and target assembly, stagnation and burn in section 3C. The locations of the diagnostics on the target chamber is discussed in section 4. The important but often overlooked target diagnostic control system is described in section 5. A comparison of NIF diagnostics with the Nova diagnostics is in section 6. The NIF diagnostic capability is broadly equivalent to Nova's in 1999. NIF diagnostics have a greater degree of automation than Nova's and in the NIF set there is some scientific innovation in DIXI.

References

- 1 J.D. Kilkenny, "Recent diagnostic developments at Nova (invited)," Rev Sci Instrum. **63**, 4688 (1992).
- 2 "National Ignition Facility Conceptual Design Report", UCRL-PROP-117093 Vol 2

NIF-LLNL-94-113 L-16973-1, May 1994.

- 3 J. D. Kilkenny et. al. Diagnostic systems for the National Ignition Facility(NIF)(Invited)", Rev. Sci. Instrum. **66**, 288 (1995).
- 4 J.D. Kilkenny, et al., "Diagnostic Development for the National Ignition Facility", Laser and Particle Beams (1997)
- 5 R. J. Leeper et. al., "Target diagnostic system for the National Ignition Facility", Rev. Sci. Instrum. **68**, 868 (1997).
- 6 T. J. Murphy et al, "Neutron time-of-flight and emission time diagnostics for the National Ignition Facility", Rev. Sci. Instrum. 72, 850 (2001).
- 7 J.D. Moody et al., "Backscatter measurements for NIF ignition targets," Rev. Sci. Instrum. 81, 10D921 (2010).
- 8 E. L. Dewald et. al., "Dante soft x-ray power diagnostic for National Ignition Facility", , Rev. Sci. Instrum. 75, 3759 (2004). K. M. Campbell et. al. "Omega Dante soft x-ray power diagnostic component calibration at the National Synchrotron Light Source" , Rev. Sci. Instrum. 75, 3768 (2004).
- 9 E.L. Dewald et al., "Hot electron measurements in ignition relevant hohlraums on the National Ignition Facility," Rev. Sci. Instrum. 81, 10D938 (2010).
- 10 M. Hohenberger et. al. "Time-resolved measurements of the hot-electron population in ignition-scale experiments on the National Ignition Facility (invited)", Rev. Sci. Instrum. 85 , 11D501 (2014)
- 11 M.B. Schneider et al., "Images of the laser entrance hole from the static x-ray imager at NIF," Rev. Sci. Instrum. **81**, 10E538 (2010).
- 12 M.B. Schneider et al., "Soft x-ray images of the laser entrance hole of ignition hohlraums," Rev. Sci. Instrum. **83**, 10E525 (2012).
- 13 P. M. Celliers, D. K. Bradley, G. W. Collins, D. G. Hicks, T. R. Boehly and W. J. Armstrong, "Line-imaging velocimeter for shock diagnostics at the OMEGA laser facility", Rev. Sci. Instrum. **75**, 4916 (2004) .
- 14 R.M. Malone et al, "Overview of the line-imaging VISAR diagnostic at the National Ignition Facility," *Proc. SPIE* **6342** (2007).
- 15 J.R. Kimbrough et al., "Standard design for National Ignition Facility x-ray streak and framing cameras," Rev. Sci. Instrum. **81**, 10E530 (2010).
- 16 Kentech Instruments Ltd, Wallingford, UK.

- 17 E.L. Dewald, et al., “Capsule Ablator Inflight Performance Measurements Via Streaked Radiography Of ICF Implosions On The NIF” Rev. Sci. Instrum. IFSA 2013 proceedings (2014).
- 18 Y.P. Opachich et al., “X-ray streak camera cathode development and timing accuracy of the 4 ω ultraviolet fiducial system at the National Ignition Facility,” Rev. Sci. Instrum. **83**, 10E123 (2012).
- 19 J. D. Kilkenny, P. Bell, R. Hanks, G. Power, R. E. Turner and J. Wiedwald, “High-speed gated x-ray imagers (invited)”, Rev. Sci. Instrum. **59**, 1793 (1988). G.A. Kyrala et al., “Measuring symmetry of implosions in cryogenic hohlraums at the NIF using gated x-ray detectors,” Rev. Sci. Instrum. **81**, 10E316 (2010).
- 20 P.M. Bell et al., “Radiation hardening of gated x-ray imagers for the National Ignition Facility,” Rev. Sci. Instrum. **81**, 10E540 (2010). N. Izumi et. al., “Experimental study of neutron induced background noise on gated x-ray framing cameras,” Rev. Sci. Instrum. **81**, 10E515 (2010)
- 21 L. R. Benedetti et. al. “Crosstalk in x-ray framing cameras: Effect on voltage, gain, and timing (invited)” Rev. Sci. Instrum. **83**, 10E135 (2012).
- 22 V. Yu Glebov et al., “The National Ignition Facility neutron time-of-flight system and its initial performance,” Rev. Sci. Instrum. **81**, 10D325 (2010).
- 23 H. G. Rinderknecht et al., “A novel particle time of flight diagnostic for measurements of shock- and compression-bang times in D³He and DT implosions at the NIF,” *Rev. Sci. Instrum.* **83**, 10D902 (2012).
- 24 H. G. Rinderknecht et. al., “A magnetic particle time-of-flight (MagPTOF) diagnostic for measurements of shock- and compression-bang time at the NIF(invited)”, Rev. Sci. Instrum. **85**, 11D901 (2014).
- 25 D. H. Edgell et al, “South pole bang-time diagnostic on the National Ignition Facility (invited)” Rev. Sci. Instrum. **83**, 10E119 (2012).
- 26 S.F. Khan et al., “Measuring x-ray burn history with the Streaked Polar Instrumentation for Diagnosing Energetic Radiation (SPIDER) at the National Ignition Facility,” *Proc. SPIE* **8505** (2012).
- 27 H.W. Herrmann et al., “Diagnosing inertial confinement fusion gamma ray physics,” *Rev. Sci. Instrum.* **81**, 10D333 (2010).
- 28 D.B. Sayre et al., “Multi-shot analysis of the gamma reaction history diagnostic,” *Rev. Sci. Instrum.* **83**, 10D905 (2012).

- 29 G. W. Cooper et al “Copper activation deuterium-tritium neutron yield measurements at the National Ignition Facility”, *Rev. Sci. Instrum.* **83**, 10D918 (2012).
- 30 C. B. Yeamans, D. L. Bleuel and L. A. Bernstein, “Enhanced NIF neutron activation diagnostics” *Rev. Sci. Instrum.* **83**, 10D315 (2012).
- 31 D.L. Bleuel et. al., “Neutron activation diagnostics at the National Ignition Facility,” *Rev. Sci. Instrum.* **83**, 10D313 (2012).
- 32 V. Smalyuk et al., “X-ray imaging in an environment with high-neutron background on National Ignition Facility” *Proc. SPIE* **8144**, 81440N (2011).
- 33 S.R. Nagel et al., “Dilation x-ray imager a new/faster gated x-ray imager for the NIF,” *Rev. Sci. Instrum.* **83**, 10E116 (2012).
- 34 D. B. Ress, R. A. Lerche, R. J. Ellis, S. M. Lane, and K. A. Nugent, “Neutron Imaging on Nova”, *Science* **241**, 956 (1988) .
- 35 L. Disdier et. al. “Neutron imaging of ICF target plasmas (invited)” *Rev. Sci. Instrum.* **74**, 1832 (2003).
- 36 “The neutron imaging diagnostic at NIF (invited)”, F. E. Merrill, et. al. ,*Rev. Sci. Instrum.* **83**, 10D317 (2012). E.N. Loomis et al., “Progress toward the development and testing of source reconstruction methods for NIF neutron imaging,” *Rev. Sci. Instrum.* **81**, 10D311 (2010).
- 37 R.A. Lerche et al., “National Ignition Facility neutron time-of-flight measurements,” *Rev. Sci. Instrum.* **81**, 10D319 (2010).
- 38 R. Tommasini et. al., “Development of Compton radiography of inertial confinement fusion implosions,” *Physics of Plasmas* **18**, 056309 (2011).
- 39 J.A. Frenje et al., “Probing high areal-density cryogenic deuterium-tritium implosions using downscattered neutron spectra measured by the magnetic recoil spectrometer,” *Physics of Plasmas* **17**, 056311 (2010).
- 40 M. Gatu Johnson et al., “Neutron spectrometry—An essential tool for diagnosing implosions at the National Ignition Facility,” *Rev. Sci. Instrum.* **83**, 10D308 (2012).
- 41 D.T. Casey et al., “The coincidence counting technique for orders of magnitude background reduction in data obtained with the magnetic recoil spectrometer at OMEGA and the NIF,” *Rev. Sci. Instrum.* **82**, 073502 (2011).

- 42 D.T. Casey et al., “Measuring the absolute deuterium–tritium neutron yield using the magnetic recoil spectrometer at OMEGA and the NIF,” *Rev. Sci. Instrum.* **83**, 10D912 (2012).
- 43 V. Yu. Glebov, C. Stoeckl, T. C. Sangster, S. Roberts, G. J. Schmid, R. A. Lerche and M. J. Moran, “Prototypes of National Ignition Facility neutron time-of-flight detectors tested on OMEGA”, *Rev. Sci. Instrum.* **75**, 3559 (2004).
- 44 V. Yu. Glebov et. al., “Testing a new NIF neutron time-of-flight detector with a bibenzyl scintillator on OMEGA” *Rev. Sci. Instrum.* **83**, 10D309 (2012).
- 45 D. A. Shaughnessy et. al., “The Radiochemical Analysis of Gaseous Samples (RAGS) apparatus for nuclear diagnostics at the National Ignition Facility (invited)” *Rev. Sci. Instrum.* **83**, 10D917 (2012).
- 46 D. A. Shaughnessey et. al. “ Radiological determination of Inertial Confinement Fusion capsule compression at the National Ignition Facility” *Rev. Sci. Instrum.* **85**, 063508 (2014)
- 47 A.B. Zylstra et al., “Charged-particle spectroscopy for diagnosing shock ρR and strength in NIF implosions,” *Rev. Sci. Instrum.* **83**, 10D901 (2012).
- 48 A.B. Zylstra et al., “The effect of shock dynamics on compressibility of ignition-scale NIF implosions”, submitted to *Phys. Plasmas*.
- 48b A.B. Zylstra et al., “In-flight observations of low-mode rR asymmetries in NIF implosions” , submitted to *Phys. Rev. E*.
- 49 T. Ma et al., “Imaging of high-energy x-ray emission from cryogenic thermonuclear fuel implosions on the NIF,” *Rev. Sci. Instrum.* **83**, 10E115 (2012).
- 50 S.P. Regan et al., “Applied plasma spectroscopy: Laser-fusion experiments,” *High Energy Density Physics* **5**, 234 (2009).
- 51 R.T. Shelton et al., “Target diagnostic control system implementation for the National Ignition Facility,” *Rev. Sci. Instrum.* **81**, 10E101 (2010).
- 52 M.S. Hutton et al., “Experiment archive, analysis, and visualization at the National Ignition Facility” *Fusion Eng. Des.* **87** (2012).